J. Fluid Mech. (2009), *vol.* 624, *pp.* 23–32.
doi:10.1017/S002211200900593X Printed in the United Kingdom

The role of superhydrophobicity in the adhesion of a floating cylinder

DUCK-GYU LEE AND HO-YOUNG KIM†

School of Mechanical and Aerospace Engineering, Seoul National University, Seoul 151-744, Korea

(Received 19 August 2008 and in revised form 9 January 2009)

Horizontal cylinders floating on liquid surfaces are mundanely observed, whose examples include the legs of aquatic arthropods and floating larvae, twigs and hairs. We study the force and energy required to lift the cylinder clear from the water surface, to evaluate the role of wettability, especially superhydrophobicity, in the adhesion of floating cylinders. We find that a drastic degree of energy saving is achieved when lifting a superhydrophobic cylinder as compared with a cylinder with moderate wettability. This can serve as a starting point to understand how the superhydrophobicity of the legs of water-walking insects help to propel them efficiently.

1. Introduction

To lift a horizontal cylinder initially floating on a liquid surface, one needs to exert force in excess of the cylinder's weight to overcome the adhesion between the solid and the liquid. Also, it is a mundane experience that less wettable solid objects need to be pulled up a shorter distance than more wettable ones before detachment, implying that less work is necessary. Here we aim to quantify the force of the adhesion and the energy required to lift the cylinder clear from the liquid surface, which are dependent on the solid wettability. Horizontal objects floating on liquid surfaces are commonly observed with the examples including hairs, fibres, minerals, twigs, bacteria and larvae (Hu & Bush 2005) floating on water. An industrial mineral-separation process called flotation (Derjaguin & Dukhin 1961) needs understanding of the physics of detachment.

Another interesting problem involving detachment of floating cylinders can be found in some insects and spiders. Aquatic arthropods, such as the water strider and the fishing spider, have such an amazing mobility on water that they float effortlessly using only tarsi, skate and even jump on water (Hu, Chan & Bush 2003; Bush & Hu 2006). In seeking to understand the relationships between these exceptional functions and the biological adaptations required to facilitate them, it was found that the surface of a water strider's legs is covered with a mat of fine, oriented hairs which themselves are covered with nanogrooves. This hierarchical structure explains the observed superhydrophobicity of the legs, which typically have a contact angle near 167° (Gao & Jiang 2004; Bush, Hu & Prakash 2008). It has also been observed that a single leg is able to support a load 15 times greater than the weight of the water strider without piercing the air–water interface (Gao & Jiang 2004). It was widely

† Email address for correspondence: hyk@snu.ac.kr

assumed that this striking load-bearing capacity is due to the superhydrophobicity of the strider's legs. However, recent experimental and theoretical studies (Vella, Lee & Kim 2006; Liu, Feng & Wang 2007; Song & Sitti 2007) have revealed that less hydrophobic (having contact angle near 90°) cylindrical rods are able to support similar maximum loads to superhydrophobic cylinders of the same dimensions. This is particularly the case for rods with small diameter (water strider legs typically have diameter 100 μm), suggesting that the superhydrophobicity of these legs can only have a limited influence on the insect's static stability at the interface.

The relative insensitivity of the leg's static load-supporting capability to the precise level of its hydrophobicity suggests that the water-repellent hairy surface of a water strider may instead play an important role in dynamic situations. Superhydrophobic surfaces immersed in liquid have been reported to experience less drag (Choi & Kim 2006); thus this mechanism may reduce the water resistance when the striders skate on water (Shi *et al.* 2007; Bush *et al.* 2008). The unique properties of these surfaces can help a submerged water strider being bombarded by raindrops to quickly resurface on water (Shi *et al.* 2007). It was also pointed out that the directionality of microsetae and nanogrooves on the legs may increase the interaction force with water while the strider propels itself (Bush *et al.* 2008). The effects of the directionality of flow slip that can be invoked by those tiny hairs on the friction force between a fluid and a boundary were quantified by Philip (1972), Lauga & Stone (2003) and Sbragaglia & Prosperetti (2007). A recent experimental study also showed that tiny superhydrophobic spheres are able to bounce off the water surface after impact – something that is not observed with less hydrophobic spheres (Lee & Kim 2008). This observation implies that strong water repellency is essential for the strider to be able to jump on water.

Although several qualitative hypotheses of how superhydrophobicity helps the life of aquatic arthropods on water have been suggested as described above, quantitative explanations of the role played by their unique water-repellent surfaces can hardly be found. Considering that a water strider should lift its legs to propel itself, the study of the detachment process of a floating cylinder can serve as a starting point to understand the role of superhydrophobicity in the strider locomotion in addition to the aforementioned practical and mundane implications. In the following, we formulate the theory to calculate the force and energy required to lift a cylinder clear from the water surface and experimentally corroborate the results.

2. Theoretical formulation and experiments

2.1. *Lifting energy*

We consider a solid cylinder of radius r_0, length L and density ρ_s being lifted off liquid having density ρ_w and surface tension γ in a quasi-static manner as shown in figure 1. The work W required to lift the cylinder off the liquid surface can be obtained by integrating the pulling force F_p along the displacement of the centre of the cylinder cross-section in the y-direction:

$$W = \int_{h_a}^{h_b} F_p \mathrm{d}y, \tag{2.1}$$

where h_a is the position of the centre of the cylinder when floating in equilibrium (i.e. when $F_p = 0$) and h_b is the elevation of the cylinder corresponding to the complete detachment of the liquid meniscus. The force balance states that F_p should be equal

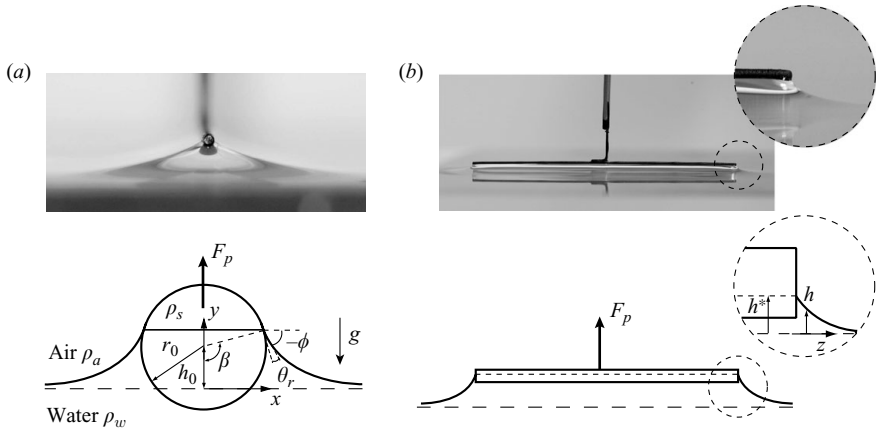

FIGURE 1. Images and schematics of a cylinder being lifted vertically off the liquid surface. (*a*) The view along the axis of the cylinder. (*b*) The view perpendicular to the axis of the cylinder. The radius, the length and the receding contact angle of the cylinder are 0.23 mm, 39.9 mm and 50°, respectively.

to the sum of the solid weight F_w, the buoyancy F_b, the surface tension force along the cylinder side F_s and the surface tension force at the ends of the cylinder F_e:

$$F_p = F_w + F_b + F_s + F_e. \tag{2.2}$$

The weight of the solid cylinder $F_w = \pi\rho_s r_0^2 g L$, where g is the gravitational acceleration. The buoyancy $F_b = \rho_w g \Omega_1$, where Ω_1 is the volume of liquid bounded by the wetted surface of the cylinder side, a vertical plane through the three-phase line and the undisturbed horizontal free surface (Keller 1998). Thus we get $\Omega_1 = r_0^2 L(2h^* \sin\beta/r_0 - \beta + \sin\beta\cos\beta)$, where h^* is the elevation of the contact line on the cylinder side and β is the angular position of the contact line as shown in figure 1. The surface tension force along the side $F_s = -2\gamma L \sin\phi$, where ϕ is the slope of the tangent of the meniscus at the cylinder side. The force at the ends of the cylinder F_e is equivalent to the weight of the liquid lifted by the cylinder ends (Keller 1998); thus $F_e = 2\rho_w g \Omega_2$, where Ω_2 is the liquid volume obtained by integrating h as shown in figure 1(*b*) over the area on the original horizontal free surface A_b: $\Omega_2 = \int_{A_b} h \mathrm{d}A_b$. For a very long cylinder in which the end effects can be neglected, $F_s \gg F_e$; then the problem reduces to a two-dimensional one, which was treated for a case $F_p = 0$ previously (Vella *et al.* 2006). For cylinders with finite length in which F_e is no longer negligible as compared with F_b, the three-dimensional Young–Laplace equation (Feng *et al.* 2007) should be solved:

$$\frac{\rho_w g}{\gamma} h = \frac{\left(1 + h_x^2\right) h_{zz} - 2h_x h_z h_{xz} + \left(1 + h_z^2\right) h_{xx}}{\left(1 + h_x^2 + h_z^2\right)^{3/2}}. \tag{2.3}$$

We employ a finite-difference method to numerically solve and integrate (2.3) over the area and determine F_e. Here we note that F_e accounts for the weight of liquid pulled along with the liquid lifted by the cylinder side near the end as shown in figure 2 which is the computed profile of the meniscus adjoining the cylinder end. Thus F_e is not simply scaled as γr_0 but rather is significantly greater than that.

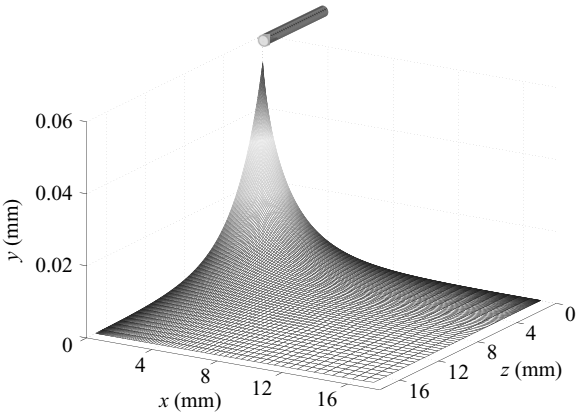

FIGURE 2. The profile of the meniscus adjoining an end of a cylinder with the radius 50 μm and $\theta_r = 160^\circ$ whose centre is lifted 0.0997 mm above the free surface (xz-plane). The cylinder axis is parallel to the z-axis, and its end faces the xy-plane. The three-dimensional Young–Laplace equation was solved assuming that h at $z = 0$ is given by the two-dimensional Young–Laplace equation solved for the cylinder side. Only half the elevated surface (positive x) is shown for clarity.

2.2. *Detachment condition*

In integrating F_p in y, it is necessary to find h_a and h_b, corresponding to the initial and end positions of the cylinder-lifting process, respectively. The initial equilibrium position h_a is obtained straightforwardly by solving (2.2) with $F_p = 0$. A condition for the liquid meniscus to detach from the solid cylinder is needed to predict h_b, which is elaborated on in the following: As the cylinder is lifted, the menisci touching the cylinder side approach each other, moving on the lower side of the cylinder. Although it is possible to theoretically calculate the meniscus profile until the two menisci eventually meet, our experiments (described below) reveal that the detachment of the liquid menisci occurs well before the menisci intersect. Thus, we employ a free energy analysis to find the detachment condition of the liquid meniscus from the solid surface. Rapacchietta, Neumann & Omenyi (1977) calculated the free energy differences at various positions of a two-dimensional, infinitely long cylinder with the reference state being the one in which the cylinder is separated from the fluid interface. We predict the detaching height h_b using the condition that upon detachment the difference of the free energy E from that of the reference detached state (E_r) vanishes: $\Delta E = E - E_r = 0$. Further elevation of the cylinder without meniscus detachment leads to a higher energy state than the reference state; thus small perturbations to the system cause the meniscus to be detached. Figure 3 illustrates the schematic meniscus profile and ΔE versus β.

Lifting a cylinder keeping contact with the liquid menisci causes the free energy change of liquid associated with the changes of the interfacial areas of the liquid with the solid (ΔE_1) and with the air (ΔE_2) and the changes of the gravitational potential energy of the liquid (ΔE_3). In principle, the surface being hysteretic, the definition of free energy associated with the change of the liquid–solid interfacial area is ambiguous. However, as the motion never changes sign, the contact angle is locked to the receding value, and we can here define an effective free surface energy difference ΔE_1 as

$$\Delta \hat{E}_1 = -2\beta \cos\theta_r - 2\frac{r_0}{L}\cos\theta_r(\beta - \sin\beta\cos\beta), \tag{2.4}$$

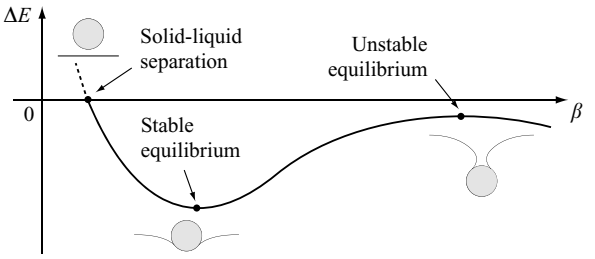

FIGURE 3. The schematic of a free energy diagram for a floating cylinder.

where the dimensionless energy $\hat{E} = E/Lr_0\gamma$ and θ_r is the receding contact angle. The first and second terms of the right-hand side of (2.4) correspond to the energy differences due to the change of the interfacial area on the cylinder side and on the cylinder ends, respectively. Here we write the free energy difference per unit area $\Delta e = \gamma_{SG} - \gamma_{SL} = \gamma\cos\theta_r$, where γ_{SG} and γ_{SL} are the interfacial energy per unit area between solid and gas and that between solid and liquid, respectively, because of the following reason: As the force exchanged between the solid and the free surface is always equal to $\gamma\cos\theta_r$, Δe is exactly equal to this value (principle of virtual works). An alternative justification can also be provided in the framework of some specific models of wetting, for instance those proposed by Blake & Haynes (1969) and de Ruijter, Blake & De Coninck (1999). In this framework, Δe consists of the difference of the equilibrium interfacial energies per unit area, $\gamma\cos\theta_e$ via Young's equation, and the work q done by the force causing the contact line to move per unit displacement of unit length. Here θ_e is the equilibrium contact angle. They suggested a microscopic model in which the movement of the contact line can be viewed as the motion of fluid molecules to the neighbouring adsorption site on a solid. The jumping of fluid molecules between the adsorption sites is caused by the out-of-balance surface tension acting on the contact line; thus the work q is written as $q = \gamma(\cos\theta_r - \cos\theta_e)$. Then we get $\Delta e = \gamma\cos\theta_r$.

The change of the air–water interfacial area causes the free energy difference $\Delta\hat{E}_2$:

$$\Delta\hat{E}_2 = \frac{2\sqrt{2}}{Bo^{1/2}}\left\{\sqrt{2} - [1-\cos(\theta_r+\beta)]^{1/2}\right\} - 2\sin\beta + 2\frac{A_i - A_b}{r_0 L}, \tag{2.5}$$

where the Bond number $Bo = \rho_w g r_0^2/\gamma$ and A_i is the interfacial area between the air and the liquid lifted by a cylinder end. The first two terms of right-hand side of (2.5) are due to the change of the interfacial area of the liquid lifted by the cylinder side with the air, and the last term is due to the change of the interfacial area of the liquid lifted by the cylinder end with the air. As the menisci are lifted with the cylinder, the gravitational potential energy of the liquid changes. The work to depress or raise the liquid volume by the cylinder side, represented as the hatched area in figure 4, causes the free energy difference $\Delta\hat{E}_{31}$:

$$\Delta\hat{E}_{31} = \frac{2}{3}\left(\frac{2}{Bo}\right)^{1/2}\left\{[1-\cos(\theta_r+\beta)]^{1/2}\,[2+\cos(\theta_r+\beta)] - \sqrt{2}\right\}. \tag{2.6}$$

The free energy change associated with the work to raise or depress the liquid underneath the cylinder, whose volume corresponds to the grey area in figure 4, is

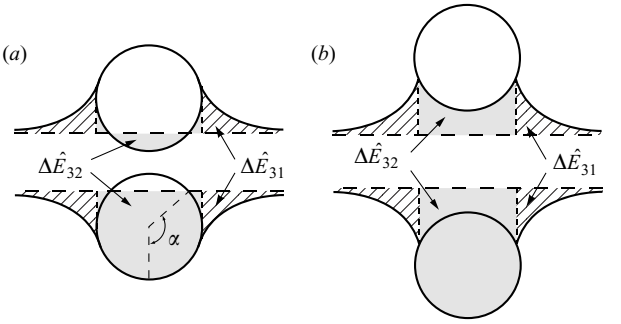

FIGURE 4. The view along the axis of the cylinder for the liquid elevated or depressed by the cylinder (*a*) for $|h_0| \leqslant r_0$ and (*b*) for $|h_0| > r_0$.

given by

$$\Delta\hat{E}_{32} = Bo\left[\cos^2\alpha\sin\beta - \left(\beta + \frac{1}{2}\sin 2\beta\right)\cos\alpha + \sin\beta - \frac{1}{3}\sin^3\beta\right] \tag{2.7}$$

for $|h_0| \leqslant r_0$ and

$$\Delta\hat{E}_{32} = Bo\left[\left(\frac{h^*}{r_0}\right)^2\sin\beta + \left(1 - \frac{1}{3}\sin^2\beta\right)\sin\beta - \beta\cos\beta - \frac{h^*}{r_0}(\beta - \sin\beta\cos\beta)\right] \tag{2.8}$$

for $|h_0| > r_0$, where α is the angular position at which the extended undeformed free surface intersects the cylinder. The last contribution to $\Delta\hat{E}_3$ comes from the work to raise or depress the volume of the liquid around the cylinder ends:

$$\Delta\hat{E}_{33} = \frac{Bo}{Lr_0^3}\int_{A_b} h^2\,\mathrm{d}A_b. \tag{2.9}$$

Thus the total free energy associated with the work to lift the liquid weight $\Delta\hat{E}_3 = \Delta\hat{E}_{31} + \Delta\hat{E}_{32} + \Delta\hat{E}_{33}$.

2.3. *Experiments*

Before discussing the results of the theoretical work to lift cylinders, we describe the experiments performed to corroborate our theory. Starting from the equilibrium position with $F_p = 0$, which is a stable equilibrium in which the total free energy change, $\Delta\hat{E} = \Delta\hat{E}_1 + \Delta\hat{E}_2 + \Delta\hat{E}_3$, is negative, we gradually lift the cylinder to find F_p as a function of h_0. When the theoretically calculated $\Delta\hat{E}$ reaches zero, the cylinder is assumed to be completely detached from the liquid surface. To verify our theory, we measured the force required to lift a floating thin cylinder off the water surface as a function of the cylinder location. In the experiments, the stainless steel wires with $r_0 = 400\,\mu\mathrm{m}$, $L = 4$ cm and $\rho_s = 8000\,\mathrm{kg\,m^{-3}}$ were coated with three different materials to vary the solid's wettability. By spray-coating the wire with a nitrocellulose lacquer (NL), we obtained the receding contact angle of $\theta_r = 50^\circ$. By dip-coating the wire with paraffin wax (PW), we obtained $\theta_r = 96^\circ$. Superhydrophobic wires were fabricated by spray-coating the wire with a mixture of melted alkyl ketene dimer (AKD) and chloroform, which resulted in $\theta_r = 148^\circ$ (Torkkeli *et al.* 2001). The receding contact angles were measured by pulling planar sheets coated with each material out of water with the same speed as used in the main experiments ($10\,\mu\mathrm{m\,s^{-1}}$). The images of the menisci were taken from the side with a camera of 512×512 pixels. The range of error

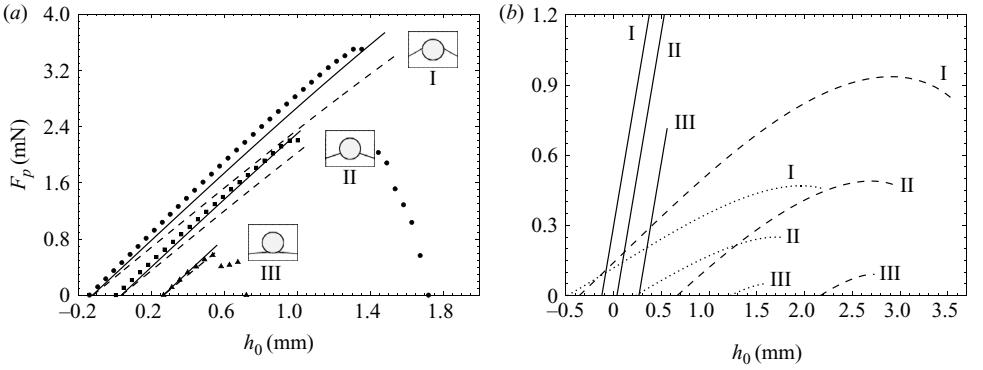

FIGURE 5. Pulling force versus cylinder elevation. (*a*) Comparison of the theoretical predictions (solid and dashed lines) and the experimental results of F_p as functions of the location of the cylinder centre. The solid lines correspond to the theoretical results considering the weight of liquid adjoining the cylinder ends (F_e) in (2.2), while the dashed lines correspond to the results neglecting the three-dimensional effects caused by F_e. The circles, squares and triangles denote the measurement results for the wires coated with NL (surface I: $\theta_r = 50°$), PW (surface II: $\theta_r = 96°$) and AKD (surface III: $\theta_r = 148°$), respectively. In the experiments, the force drops suddenly after reaching the maximum because the meniscus-detaching process ensues. The insets show the meniscus profiles corresponding to the moment of detachment for each contact angle condition. (*b*) Comparison of theoretical pulling forces for the cylinders (solid lines) used in (*a*), the spheres with the same surface area (dashed lines) and the spheres with the same volume (dotted lines) as those of the cylinders.

in the contact angle measurement is $\pm 1°$. To measure the force exerted on a wire in contact with water surface, we used a surface tension meter (Data Physics DCAT21), in which the wire was fixed on a balance located at the top of the apparatus, and the water vessel moved down at the rate $10\,\mu\mathrm{m\,s^{-1}}$. The errors associated with reading the position and the force are within $\pm 0.1\,\mu\mathrm{m}$ and $\pm 0.1\,\mu\mathrm{N}$, respectively.

3. Results

The force measurement results are compared with the theory in figure 5(*a*). The theoretical force values considering the liquid weight adjoining the cylinder ends as well as the cylinder side agree well with the experimental results, while the two-dimensional model excluding the liquid weight surrounding the cylinder ends exhibits increasing discrepancy with the experiments with the increase of h_0. Furthermore, the theory predicts the cylinder height, where the liquid menisci are detached from the solid fairly accurately. On the other hand, a simplistic hypothesis that the cylinder is detached clear from water when the two hanging menisci intersect each other predicts detachment heights which are approximately four times greater than those obtained from the free energy analysis above ($h_b = 5.17\,\mathrm{mm}$ for an NL cylinder, $h_b = 3.88\,\mathrm{mm}$ for a PW cylinder and $h_b = 1.78\,\mathrm{mm}$ for an AKD cylinder, using the simplistic detachment hypothesis). We find that the more hydrophobic the cylinder, the smaller the area below the force curve which corresponds to the work required to lift each cylinder off the liquid surface. This considerable reduction of lifting energy with the increased hydrophobicity is caused by the fact that a more hydrophobic cylinder floats higher initially with a smaller area being wetted (the force curve starting from higher h_0) and that the liquid menisci are detached from the cylinder earlier (the force curve ending at lower h_0).

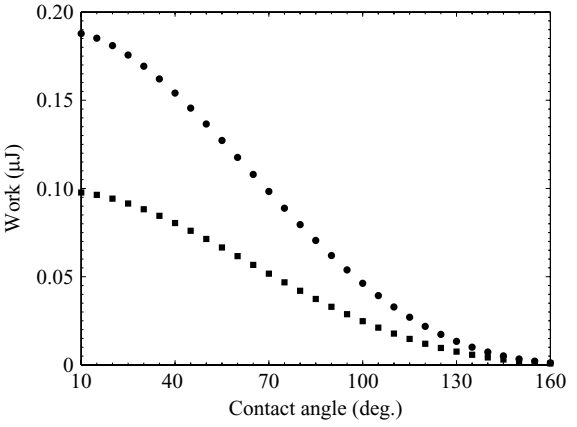

FIGURE 6. The work required to lift a cylinder having the characteristic dimensions of a water strider's leg, $L = 5.5\,\text{mm}$ and $r_0 = 60\,\mu\text{m}$, for different contact angles. The circles denote the theoretical results considering the three-dimensional effect due to the meniscus at the cylinder end, and the squares correspond to the two-dimensional results neglecting the cylinder end effects. Although the two models predict slightly different detachment height, we used the same detachment height for both the calculations that was from the three-dimensional model.

Figure 5(*b*) compares the pulling force for the three-dimensional cylinder of figure 5(*a*) with the forces required to pull the spheres with the same volume and with the same surface area as those of the cylinder. The force components due to buoyancy and surface tension and the free energy change associated with the sphere-lifting process are given by Rapacchietta & Neumann (1977). We used the same criterion for the meniscus detachment, i.e. $\Delta E = 0$, for the spheres. The forces to pull the spheres are shown to be considerably less than that for the cylinders. This is primarily due to reduced contact line length of the spheres which determines the magnitude of the surface tension force. The sphere of the same volume as that of a cylinder with $L \gg r_0$ has the radius $r_V \sim (r_0^2 L)^{1/3}$. Thus the ratio of the contact line length of the sphere l_V and that of the cylinder l_C becomes $l_V/l_C \sim (r_0/L)^{2/3}$. For the sphere of the same surface area with the radius $r_A \sim (r_0 L)^{1/2}$, the ratio of the contact line length of the sphere l_A and l_C is $l_A/l_C \sim (r_0/L)^{1/2}$. Figure 5 shows that the sphere with the same volume needs less pulling force than the sphere with the same surface area, a tendency consistent with $l_V/l_C < l_A/l_C$.

Our general theory to predict the force and energy to detach a cylinder from the water surface can be applied to a biologically relevant situation. Considering that the legs of water striders are superhydrophobic, we compare the energy values required to lift legs having the characteristic dimensions of a leg of a water strider *Gerridae* (Hu 2006), $L = 5.5\,\text{mm}$ and $r_0 = 60\,\mu\text{m}$, with varying wettability. Integrating the pulling force to lift the leg until the menisci are detached for different contact angles leads to the results as shown in figure 6. The figure shows a dramatic reduction of energy when the leg becomes hydrophobic: the required work is 1.21 nJ for $\theta_r = 160^\circ$, only 1.96 % and 5.55 % of the work required for $\theta_r = 90^\circ$ and 120°, respectively. Hu (2006) measured the leaping height of a 4.5 mg heavy water strider to be 5 cm, to find that the associated potential energy increase reaches 2.2 μJ, giving a characteristic value of work per stroke in the strider propulsion. Considering that the strider's six legs are wet over the perimeter of 22 mm, the values of the energy required to lift the legs of the same size off water but with the contact angle 10° and 90° are 0.75 μJ

(34 % of the characteristic work) and 0.25 μJ (11 % of the characteristic work), respectively. However, when the contact angle increases to 160°, the lifting energy becomes as small as 4.85 nJ, only 0.22 % of the characteristic work. Although our analysis oversimplifies the real motion of the water strider legs as discussed below, the foregoing calculation suggests that the strider with water-repellent legs can avoid wasting energy to overcome the legs' adhesion with water in a routine life of skating and jumping.

4. Discussion

The theory that was developed and experimentally corroborated in this work enabled us to calculate the work needed to lift horizontal cylinders clear from the water surface. The superhydrophobicity of the cylinder was shown to dramatically reduce the detachment work, and the degree of energy saving was quantified. In addition to providing an analytical tool to understand the mundane phenomena of wet adhesion of floating objects, our work can be employed to understand an industrial mineral-separation process, flotation, and the biological locomotion associated with aquatic arthrodpods with some limitations as discussed below. As the biologically inspired robotic technology advances rapidly (Hu *et al.* 2007), our theory can also be applied to predicting the driving power of the robots mimicking the aquatic arthropods that seem to have been evolved to save energy so efficiently.

Although our current theory can be applied to understand a role of the superhydrophobicity in the aquatic arthropod locomotion, our focus has been on a quasi-static process of vertical lifting; much remains to be done to further the understanding of the role of super-water-repellent hairy structure of the water strider's leg in more realistic locomotion scenarios. Firstly, dynamic effects associated with the motion of the leg and the surrounding fluid need to be added when the leg moves with a velocity U that is no longer negligible. Then the force balance should include the inertia of the leg ($\sim\rho_s r_0^2 L\dot{U}$) and of the surrounding water ($\sim\rho_w r_0^2 L\dot{U}$), viscous friction ($\sim(\rho_w \mu r_0 L^2 U^3)^{1/2}$) and form drag ($\sim\rho_w U^2 r_0 L$), where the overdot denotes the time derivative and μ is the water viscosity. Furthermore, the dynamic meniscus shape no longer follows the Young–Laplace equation and must be calculated by solving for the full fluid flow problem, as has recently been done for the impact of a small object onto a liquid surface (Vella & Metcalfe 2007). This dynamic evolution will alter the volume and the interfacial area of liquid dragged upward by the rising solid. Secondly, one needs to consider a case in which a water strider lifts its legs oblique rather than perpendicular to the horizontal, especially when skating. Bush *et al.* (2008) postulated that the water strider withdraws its leg after the driving stroke in such a direction that a peeling of the tilted flexible nanohairs covering the leg occurs. Then the directional wettability of the leg may play an important role. One also needs to consider the fact that the water strider leg surface is covered by a series of hairs that are inclined relative to the leg, bending so as to lie roughly parallel to the leg axis. The sum of the detachment force on an individual hair would be the total force experienced by a leg, and the smooth cylinder approach as adopted here may be valid only when the spacing between hairs is sufficiently small.

We thank Dr Dominic Vella for stimulating discussions. This work was supported by Korea Research Foundation grants (KRF-2006-331-D00068 and KRF-2007-412-J03001) administered via SNU-IAMD.

REFERENCES

Blake, T. D. & Haynes, J. M. 1969 Kinetics of liquid/liquid displacement. *J. Colloid Interface Sci.* **30**, 421–423.

Bush, J. W. M. & Hu, D. L. 2006 Walking on water: biolocomotion at the interface. *Annu. Rev. Fluid Mech.* **38**, 339–369.

Bush, J. W. M., Hu, D. L. & Prakash, M. 2008 The integument of water-walking arthropods: form and function. *Adv. Insect Physiol.* **34**, 117–192.

Choi, C.-H. & Kim, C.-J. 2006 Large slip of aqueous liquid flow over a nanoengineered superhydrophobic surface. *Phys. Rev. Lett.* **96**, 066001.

Derjaguin, B. V. & Dukhin, S. S. 1961 Theory of flotation of small and medium size particles. *Trans. Inst. Mining Met.* **70**, 221–246.

Feng, X.-Q., Gao, X., Wu, Z., Jiang, L. & Zheng, Q.-S. 2007 Superior water repellency of water strider legs with hierarchical structures: experiments and analysis. *Langmuir* **23**, 4892–4896.

Gao, X. & Jiang, L. 2004 Water-repellent legs of water striders. *Nature* **432**, 36.

Hu, D. L. 2006 The hydrodynamics of water-walking insects and spiders. PhD thesis, Massachusetts Institute of Technology, Cambridge, Massachusetts.

Hu, D. L. & Bush, J. W. M. 2005 Meniscus-climbing insects. *Nature* **437**, 733–736.

Hu, D. L., Chan B. & Bush, J. W. M. 2003 The hydrodynamics of water strider locomotion. *Nature* **424**, 663–666.

Hu, D. L., Prakash, M., Chan, B. & Bush, J. W. M. 2007 Water-walking devices. *Exp. Fluids* **43**, 769–778.

Keller, J. B. 1998 Surface tension force on a partly submerged body. *Phys. Fluids* **10**, 3009–3010.

Lauga, E. & Stone, H. A. 2003 Effective slip in pressure-driven Stokes flow. *J. Fluid Mech.* **489**, 55–77.

Lee, D.-G. & Kim, H.-Y. 2008 Impact of a superhydrophobic sphere onto water. *Langmuir* **24**, 142–145.

Liu, J.-L., Feng, X.-Q. & Wang, G.-F. 2007 Buoyant force and sinking conditions of a hydrophobic thin rod floating on water. *Phys. Rev.* E **76**, 066103.

Philip, J. 1972 Flows satisfying mixed no-slip and no-shear conditions. *Z. Angew. Math. Phys.* **23**, 353–372.

Rapacchietta, A. V. & Neumann, A. W. 1977 Force and free-energy analyses of small particles at fluid interfaces. ii. spheres. *J. Colloid Interface Sci.* **59**, 555–567.

Rapacchietta, A. V., Neumann, A. W. & Omenyi, S. N. 1977 Force and free-energy analyses of small particles at fluid interfaces. i. cylinders. *J. Colloid Interface Sci.* **59**, 541–554.

de Ruijter, M. J., Blake, T. D. & De Coninck, J. 1999 Dynamic wetting studied by molecular modeling simulations of droplet spreading. *Langmuir* **15**, 7836–7847.

Sbragaglia, M. & Prosperetti, A. 2007 A note on the effective slip properties for microchannel flows with ultrahydrophobic surfaces. *Phys. Fluids* **19**, 043603.

Shi, F., Niu J., Liu, J., Liu F., Wang, Z., Feng, X.-Q. & Zhang, X. 2007 Towards understanding why a superhydrophobic coating is needed by water striders. *Adv. Mater.* **19**, 2257–2261.

Song, Y. S. & Sitti, M. 2007 Surface-tension-driven biologically inspired water strider robots: theory and experiments. *IEEE Trans. Robot.* **23**, 578–589.

Torkkeli, A., Saarilahti, J., Haara, A., Harma, H., Soukka, T. & Tolonen, P. 2001 Electrostatic transportation of water droplets on superhydrophobic surfaces. In *Proc. of the 14th IEEE Intl Conf. on MEMS*, Interlaken, Switzerland.

Vella, D., Lee, D.-G. & Kim, H.-Y. 2006 The load supported by small floating objects. *Langmuir* **22**, 5979–5981.

Vella, D. & Metcalfe, P. D. 2007 Surface tension dominated impact. *Phys. Fluids* **19**, 072108.